Zinc finger protein 514 promotes esophageal cancer progression by enhancing cell proliferation, migration and invasion

LIN LV[1,2*], XIAOMING SUN[1*], HOULU ZHANG[3], GUANGXU WANG[3], CHAO ZHANG[4], HAIBO LIU[1] and LIANGMING ZHU[1,2,5]

[1]Department of Thoracic Surgery, Jinan Central Hospital, Shandong University, Jinan, Shandong 250013, P.R. China; [2]Department of Thoracic Surgery, Medical Integration and Practice Center, Shandong University, Jinan, Shandong 250013, P.R. China; [3]School of Clinical Medicine, Shandong Second Medical University, Weifang, Shandong 261000, P.R. China; [4]Graduate Department, Shandong First Medical University, Jinan, Shandong 250000, P.R. China; [5]Department of Thoracic Surgery, Qilu Hospital, Shandong University, Jinan, Shandong 250013, P.R. China

Received March 27, 2025; Accepted September 22, 2025

DOI: 10.3892/mmr.2025.13724

Abstract. Esophageal cancer (EC), a malignant tumor occurring in the upper gastrointestinal tract, is the seventh most common cancer worldwide. Zinc finger proteins (ZNFs), the most abundant family of transcription factors in humans, serve an important role in the initiation and progression of various malignant tumors. However, the function of ZNFs in EC remains unclear. The present study aimed to elucidate the role of ZNF514 in the development and progression of EC and to investigate its underlying mechanism. The mRNA and protein expression levels of ZNF514 were assessed using reverse transcription-quantitative PCR and western blotting. To assess functional roles, multiple cellular assays were performed, including 5-ethynyl-2'-deoxyuridine incorporation, Cell Counting Kit-8, wound healing, colony formation and Transwell assays. Subsequently, for transcriptomics analysis, Gene Ontology and Kyoto Encyclopedia of Genes and Genomes analyses, Gene Set Enrichment Analysis and Ingenuity Pathway Analysis (IPA) were performed. In EC, ZNF514 exhibited high expression at both the mRNA and protein levels. Additionally, ZNF514 influenced the migration, invasion and proliferation of EC cells. Gene enrichment analyses and IPA demonstrated that ZNF514 knockdown significantly affected multiple signaling pathways, such as Fcγ receptors, the complement system, G-protein coupled receptors (GPCRs)-related receptors, the ribosomal S6 kinase (RSK) pathway, Ras/MEK, PI3K/AKT, STAT3, nucleotide-binding oligomerization domain-containing protein (NOD) and NF-κB pathways. In conclusion, the present study indicated that the anticancer mechanisms induced by ZNF514 knockdown may be related to the enhancement of Fcγ receptor and complement system activation, as well as the inhibition of GPCR, RSK, Ras/MEK, PI3K/AKT, STAT3, NOD1/2 and NF-κB pathways.

Correspondence to: Dr Liangming Zhu, Department of Thoracic Surgery, Medical Integration and Practice Center, Shandong University, 44 Wenhua West Road, Jinan, Shandong 250013, P.R. China
E-mail: 201999000028@sdu.edu.cn

Mr. Haibo Liu, Department of Thoracic Surgery, Jinan Central Hospital, 105 Jie Fang Road, Jinan, Shandong 250013, P.R. China
E-mail: lhb801103@126.com

*Contributed equally

Key words: zinc finger protein 514, esophageal cancer, Ingenuity Pathway Analysis, Ras/MEK, PI3K/AKT

Introduction

Esophageal cancer (EC) is the seventh most common cancer globally, with ~470,000 new cases diagnosed annually; In addition, EC ranks among the top in terms of incidence among upper gastrointestinal tumors (1). It has been reported that ~90% of EC cases are squamous cell carcinoma, with most of the remaining cases being adenocarcinoma (2). Owing to the absence of early-stage clinical manifestations, EC is frequently diagnosed in the advanced stages. Despite notable advancements in cancer diagnostics and treatment, with a 5-year survival rate of <30%, the clinical prognosis of EC remains poor (3). Therefore, the discovery of effective targets for the treatment and early diagnosis of EC is of great importance.

Zinc finger proteins (ZNFs), encoded by ~5% of the human genome, form the largest family of transcription factors in humans. Characterized by their finger-like DNA-binding motifs, ZNFs exert important biological functions across multiple cellular processes (4). Zinc finger motifs are currently categorized into eight major types: C2H2, TAZ2 domain-like, zinc ribbon, treble clef, Zn2/Cys6 (5), zinc-binding loop, Gag knuckle and metallothionein (6). A notable body of literature has documented the biological processes associated with ZNFs in various types of cancer. For example, ZNF322A promotes cell proliferation, motility and invasive ability in lung cancer through transcriptional activation of cyclin D1 and α-adducin, coupled with inhibition of p53. Furthermore, multivariate Cox

regression analysis has revealed that ZNF322A has a notable impact on the prognosis of lung cancer (7). Moreover, activating the PI3K/AKT pathway induces the ZNF139-mediated promotion of bladder cancer cell proliferation, motility and invasion (8). ZNF148 promotes breast cancer progression by activating microRNA-335 and superoxide dismutase 2 to enhance the production of reactive oxygen species, which further triggers pyroptotic cell death (9). To the best of our knowledge, no studies have yet reported on the prognostic relevance of ZNF514 in pan-cancer and EC analyses. Therefore, the impact of ZNF514 on the development of EC warrants further investigation.

The impact of ZNF514 on the proliferation, motility and invasiveness of EC cells was evaluated through knockdown and overexpression experiments using Kyse-150 and Kyse-510 cells. By using RNA sequencing (RNA-seq) analysis, followed by Gene Ontology (GO) and Kyoto Encyclopedia of Genes and Genomes (KEGG) analyses, Gene Set Enrichment Analysis (GSEA) and Ingenuity Pathway Analysis (IPA), the potential mechanisms underlying the functions of ZNF514 were further explored in the present study. The present study aimed to explore the pro-tumorigenic role of ZNF514 upregulation in EC, aiming to identify new therapeutic targets for EC and provide novel strategies for the diagnosis and subsequent treatment of EC.

Materials and methods

Bioinformatics analysis. The Tumor Immune Estimation Resource (TIMER; https://cistrome.shinyapps.io/timer/) database was used to detect ZNF514 upregulation across multiple malignancies. Data from patients with EC were obtained from TCGA (https://gdc-portal.nci.nih.gov), including RNA-seq data from 197 samples (184 EC tissues and 13 normal esophageal tissues). From these, 13 normal tissue samples and their paired 13 cancer tissue samples were selected, and Wilcoxon signed-ranks analysis were used to evaluate the differential expression between the two groups, and data visualization was performed using the 'ggplot2' (v3.5.1; ggplot2.tidyverse.org) package in R (v4.2.2) (https://cran.r-project.org/src/base/R-4/R-4.2.2.tar.gz). The frequency of ZNF514 gene alterations was analyzed using the cBioPortal database (www.cbioportal.org). Data and samples were retrieved from the esophageal carcinoma section of two TCGA-derived databases: Firehose legacy) (gdac.broadinstitute.org/) and TCGA (Nature 2017) (10).

Patients and specimens. Between November 2024 and January 1, 2025, six pairs of EC samples and their corresponding adjacent non-cancerous tissues were collected at Jinan Central Hospital (Jinan, China). The inclusion criteria in the present study were as follows: i) Pathological biopsy confirms esophageal cancer); ii) patients had complete pathological data; iii) patients provided written informed consent; and iv) patients did not receive any radiotherapy, immunotherapy or chemotherapy before surgery. The six pairs of cancerous samples and their corresponding adjacent non-cancerous tissues were immediately frozen to preserve freshness for subsequent western blot analysis. The protocol for the present study received approval from the Ethics Committee of Jinan Central Hospital (Jinan, China), under ethical approval number 20241120027. All procedures were conducted following applicable guidelines and regulations.

Cell lines and cell culture. The Het-1a, Kyse-30, Kyse-450, Kyse-150 and Kyse-510 cells were supplied by Shandong Provincial Hospital Affiliated to Shandong First Medical University (Jinan, China). Het-1a cells were cultured in DMEM (Gibco; Thermo Fisher Scientific, Inc.) containing 10% FBS (Hysigen). 10% FBS was added to RPMI 1640 medium (Gibco; Thermo Fisher Scientific, Inc.) for the remaining cell culture. All cell cultures were maintained at 37˚C in a humidified incubator with 5% CO_2.

Transfection. Kyse-150 (interference) and transfected overexpression plasmids into the Kyse-510 (overexpression) cell line, which were pre-cultured in 6-well plates with suitable growth medium. ZNF514 small interfering (si)RNA (Beijing Tsingke Biotech Co., Ltd.) or overexpression plasmids (Guangzhou RiboBio Co., Ltd.) were transfected using Lipofectamine 3000 (Invitrogen; Thermo Fisher Scientific, Inc.) and p3000 (Guangzhou RiboBio Co., Ltd.). siRNA was transfected using Lipofectamine 3000 alone, while plasmids were transfected using both Lipofectamine 3000 and p3000. A total of 2.5 μg siRNA was mixed with 5 μl Lipofectamine 3000 to form a Lipofectamine-siRNA complex. Alternatively, 2.5 μg of plasmid was mixed with 5 μl of Lipofectamine 3000 and 5 μl P3000 to prepare a Lipofectamine-P3000-ZNF514 plasmid complex. After incubating the complexes at room temperature for 15 min, they were added to the cells. Following transfection at 37˚C for 8 h, the medium was replaced. The cells were then further incubated at 37˚C for 24-48 h before RNA or protein extraction was performed. siRNA sequences targeting ZNF514 were as follows: si-ZNF514-1: Forward 5'-CCCUUAGCAGAGAUUAUAA-3' and Reverse 5'-UUAUAAUCUCUGCUAAGGG-3'; si-ZNF514-2: Forward 5'-GGUCACACUUCAUCCCUUA-3' and Reverse 5'-UAAGGGAUGAAGUGUGACC-3' and si-ZNF514-3: Forward 5'-GGGCCUUCUAGUAUCCAAA-3' and Reverse 5'-UUUGGAUACUAGAAGGCCC-3'. The negative control sequences were: Forward 5'-UUCUCCGAACGUGUCACGUTT-3' and reverse 5'-ACGUGACACGUUCGGAGAATT-3'. The negative control for siRNA transfection is non-targeting siRNA. In the overexpression experiment, both the ZNF514 overexpression plasmid and the control plasmid (empty pcDNA3.1 plasmid) used pcDNA3.1 as the vector backbone.

RNA extraction and reverse transcription-quantitative PCR (RT-qPCR). Total RNA was extracted from Het-1a, Kyse-30, Kyse-450, Kyse-150 and Kyse-510 cells using TRIzol® reagent (Invitrogen; Thermo Fisher Scientific, Inc.). RT of 1 μg mRNA into cDNA was performed using the Evo M-MLVRT Mix Kit Ver.2 (Hunan Accurate Biotechnology Co., Ltd.), according to the manufacturer's instructions. Gene expression was quantified with SYBR Green PCR (Hunan Accurate Biotechnology Co., Ltd.) using 10 ng cDNA as the template. Thermocycling conditions were as follows: Initial pre-denaturation at 95˚C for 30 sec, followed by 40 cycles of a denaturation step at 95˚C for 30 sec, an annealing step at 55˚C for 30 sec, and extension step at 72˚C for 30 sec. The primers used were as follows:

ZNF514, forward 5'-ACAAATCTGCCACCACCCTTA-3', reverse 5'-TGTTTCCCCCTAAAGTCTGCC-3'; and GAPDH, forward 5'-GCACCGTCAAGGCTGAGAAC-3' and reverse 5'-TGGTGAAGACGCCAGTGGA-3' (Azenta US, Inc.). Expression levels were normalized to GAPDH and analyzed using the $2^{-\Delta\Delta Cq}$ method (11).

Western blotting. Het-1a, Kyse-30, Kyse-450, Kyse-150 and Kyse-510 cells were lysed in RIPA buffer (Beijing Solarbio Science & Technology Co., Ltd.) containing protease/phosphatase inhibitors. Protein concentration was determined using a BCA kit (Beyotime Institute of Biotechnology) to ensure equal loading and the protein samples were mixed with sample buffer and heated at 98˚C for 5 min. 25 μg quantified protein lysate per lane was separated by 10% SDS-PAGE gel electrophoresis and transferred to PVDF membranes. The membranes were blocked in 0.1% TBST containing 5% non-fat milk for 1 h at room temperature, then incubated overnight at 4˚C with primary antibodies diluted in 0.1% TBST buffer. The primary antibodies used included rabbit polyclonal anti-ZNF514 antibody (1:2,000; cat. no. YT6669; ImmunoWay Biotechnology Company) and rabbit polyclonal anti-GAPDH antibody (1:10,000; cat. no. bs-2188R; Beijing Biosynthesis Biotechnology Co., Ltd.). Subsequently, the membranes were incubated with HRP-conjugated goat anti-rabbit secondary antibody (1:10,000; cat. no. bs-0295G-HRP Beijing Biosynthesis Biotechnology Co., Ltd.) at room temperature for 1 h and detected using enhanced chemiluminescence reagents (MilliporeSigma). Immunoreactive bands were visualized using a Tanon 5200 imaging system (Molecular Devices, LLC) and analyzed with ImageJ software (version 1.8.0; National Institutes of Health).

Immunohistochemistry (IHC). Esophageal cancer tissue samples collected were fixed in 4% paraformaldehyde at room temperature for 24 h, then embedded in paraffin and cut into 3-μm-thick paraffin sections. The sections were deparaffinized with xylene, followed by rehydration in a graded ethanol series. Subsequently, the sections were immersed in 1x citrate buffer (pH 6.0), heated to boiling using a pressure cooker, and then cooled to room temperature. Next, the sections were washed 3 times with PBS, 5 min each time. They were then placed in 3% hydrogen peroxide solution and incubated at room temperature for 25 min in the dark, followed by 3 washes with PBS (5 min per wash). 3% BSA (cat. no. GC305010; Servicebio) was added dropwise to cover the tissue evenly, and the sections were blocked at room temperature for 30 minutes. The sections were incubated overnight at 4˚C with rabbit polyclonal anti-ZNF514 antibody (1:200; cat. no. YT6669; ImmunoWay Biotechnology Company). After that, HRP-conjugated goat anti-rabbit secondary antibody (1:200; cat. no. GB23303; Servicebio) was added at room temperature for 50 min. Thereafter, the slides were stained with DAB (cat. no. G1212; Servicebio) and counterstained with hematoxylin at room temperature for 3 min. The sections were dehydrated, cleared, and mounted with neutral mounting medium. Finally, observations were made under a light microscope.

EdU assay. Kyse-150 and Kyse-510 cells were plated into 96-well plates at a density of $2x10^4$ cells/well and incubated for 24 h. Cell proliferation was evaluated using the EdU assay kit (cat. no. C0071S; Beyotime Institute of Biotechnology) according to the manufacturer's instructions. Briefly, cells were treated with 10 μM EdU at 37˚C for 3 h, fixed in 4% paraformaldehyde at room temperature for 10 min, permeabilized with 0.3% Triton X-100 at room temperature for 10 min, and sequentially stained with Azide 488 for 30 min and Hoechst 33342 for 10 min at room temperature. Fluorescence imaging was performed using a fluorescence microscope (Olympus Corporation) to visualize EdU-positive (proliferating) cells and total nuclei.

Cell Counting Kit (CCK)-8 cell proliferation assay. Kyse-150 and Kyse-510 cells in the exponential growth phase were seeded into 96-well plates at a density of 2,000 cells per well. At 24, 48, 72, and 96 h after cell adhesion, 10 μl of CCK-8 reagent (cat. no. BA00208; Beijing Biosynthesis Biotechnology Co., Ltd.) was added to each well, respectively. After incubation at 37˚C for 2 h, the optical density (OD) values were measured at a wavelength of 450 nm using a microplate reader (Model Spectra Max i3x; Molecular Devices).

Wound healing assay. Kyse-150 and Kyse-510 cells were seeded into 6-well plates and cultured in medium containing 10% FBS until reaching 95% confluence. Uniform scratches were created using sterile pipette tips, after which the cells were incubated in serum-free medium at 37˚C. Images were captured via phase-contrast microscope at 0 and 24 h to monitor scratch healing. Quantitative analysis of scratch healing was performed using ImageJ software [(version 1.8.0); NIH, USA], and the cell migration rate (%) was calculated using the formula: [(initial scratch width-final scratch width)/initial scratch width] x100. Finally, observations were made under a light microscope.

Colony formation assay. Kyse-150 and Kyse-510 cells were plated in 6-well plates at a density of $2x10^3$ cells/well. The culture medium was replaced every 3 days; after 14 days of incubation, the colonies were fixed with 4% paraformaldehyde for 30 min at room temperature, stained with hematoxylin (Beijing Solarbio Science & Technology Co., Ltd.) for 20 min at room temperature, scanned and counted manually. Clones were defined as colony composed of >50 cells.

Transwell assays. Transwell assays were performed in 24-well plates. For the migration assay, $2x10^4$ Kyse-150 or Kyse-510 cells were resuspended in serum-free medium and seeded into uncoated Transwell chambers (pore size, 8 μm; Corning, Inc.), with the lower chamber containing medium supplemented with 10% FBS. In the invasion assay, Transwell chambers were pre-coated with Matrigel and incubated at 37˚C for 1 h. Subsequently, $2x10^4$ cells were seeded into the upper chamber, while the lower chamber was filled with medium supplemented with 10% FBS. After incubation at 37˚C for 24-48 h, non-migrated/non-invaded cells on the upper surface of the membrane were removed. Cells that had invaded to the lower surface were fixed with 4% paraformaldehyde and stained with 0.1% crystal violet at room temperature for 15 min. Finally, observations were made under a light microscope.

RNA-seq. Total RNA was extracted from Kyse-150 cells using the MJzol Animal RNA Extraction kit (cat. no.T102096; MagBeads) in accordance with the manufacturer's instructions. RNA integrity was assessed by determining the RNA Integrity Number using an Agilent 4200 TapeStation (Agilent Technologies, Santa Clara, CA, USA). Qualified total RNA was purified using the RNAClean XP Kit (cat. no. A63987, Beckman Coulter, Inc.) and the RNase-Free DNase Set (cat. no. 79254, QIAGEN, GmbH). Subsequently, the purified total RNA underwent mRNA isolation, fragmentation, first-strand cDNA synthesis, second-strand cDNA synthesis, end repair, 3'-end adenylation, adapter ligation, and enrichment steps, following the protocol provided with the Dual-mode mRNA Library Prep Kit (cat. no. 12310ES96, YEASen). The resulting products were purified using HieffNGS DNA Selection Beads (cat. no. 12601ES56, YEASen). Library concentration was quantified using the ExKubit dsDNA HS Assay kit (cat. no. NGS00-3012, Excell) and a Qubit® 2.0 Fluorometer, while library size was determined using an Agilent 4200 TapeStation (Agilent Technologies) and diluted to 2 nM loading concentration. Sequencing was performed on an Illumina NovaSeq 6000 platform using a paired-end 150 bp mode.

Data analysis for gene expression. Raw sequencing reads underwent preprocessing to remove ribosomal RNA reads, sequencing adapters, short-fragment sequences and other low-quality reads. The cleaned reads were then mapped to the human hg38 reference genome using HISAT2 (version 2.0.4; http://daehwankimlab.github.io/hisat2/), allowing for up to two mismatches. Following genome alignment, StringTie (version 1.3.0; https://ccb.jhu.edu/software/stringtie/) was employed with reference annotation to calculate fragment per kilobase of transcript per million mapped reads (FPKM) values for known gene models. Differential gene analysis between samples was performed using edgeR (https://bioconductor.org/packages/release/bioc/html/edgeR.html) (12). After obtaining P-values, multiple hypothesis testing correction was conducted. The threshold for P-values was determined by controlling the False Discovery Rate (FDR) (13), and the corrected P-values were referred to as q-values, with fold-changes estimated based on FPKM values across samples. Significant DEGs were identified as those with a FDR value above the threshold (Q<0.05) (When the total number of DEGs in all comparisons is less than 50, the threshold will be automatically adjusted to a P-value ≤0.05) and fold-change >2 (or $|\log_2(\text{fold-change})|>1$). DEGs with a $|\log_2(\text{Fold-change})|>2$ and P<0.05 were uploaded to the STRING database (string-db.org/) to construct protein-protein interaction (PPI) networks. A high-confidence threshold, indicated by an interaction score of >0.9, was applied to filter significant protein interactions and generate the PPI network. To identify the enriched biological processes, molecular functions, and cellular components, Gene Ontology analysis (GO; http://www.geneontology.org/) was conducted. Kyoto Encyclopedia of Genes and Genomes analysis (KEGG; clusterProfiler 3.10.1; https://biocon ductor.org/packages/release/bioc/html/clusterProfiler.html) was applied to detect cellular biochemical processes closely associated with the DEGs. To identify signaling pathways significantly associated with ZNF514 expression levels, we performed Gene Set Enrichment Analysis (GSEA; https://www.gsea-msigdb.org/gsea/index.jsp).

IPA. Canonical pathway analysis and upstream regulator analysis for various DEGs were performed using IPA. (QIAGEN Inc.; https://digitalinsights.qiagen.com/IPA). In enrichment analysis, we use the z-score to quantify the degree of deviation in the overall activation/inhibition trend of a pathway. The formula:

$$Z = \frac{X - \mu}{\sigma}$$

where X represents the raw data, μ denotes the mean, and σ is standard deviation. The direction of the z-score indicates the activation or inhibition trend of the pathway, while the absolute value of the z-score reflects the significance level. Additionally, we use -log(P-value) to enhance the visual distinguishability of 'significant differences'. Specifically, a larger -log(P-value) corresponds to a smaller P-value, which in turn means the statistics are more reliable.

Statistical analysis. Data are presented as the mean ± standard deviation of at least three independent experiments. A paired-samples t-test was used to compare differences between two paired groups, while an unpaired t-test was applied to analyze differences between two independent samples. For comparisons involving more than two groups, a one-way analysis of variance was employed, followed by Dunnett's post-hoc test. P<0.05 was considered to indicate a statistically significant difference. All analyses were performed using Prism v8.0 software (Dotmatics). To quantify the linear association between two continuous variables, the Pearson correlation coefficient was calculated following standard statistical protocols. For two variables X and Y with a total sample size of n, the Pearson correlation coefficient was computed using the formula:

$$r = \frac{\sum_{i=1}^{n}(x_i - \bar{x})(y_i - \bar{y})}{\sqrt{\sum_{i=1}^{n}(x_i - \bar{x})^2}\sqrt{\sum_{i=1}^{n}(y_i - \bar{y})^2}}$$

Results

ZNF514 is upregulated in EC. The TIMER database was used to investigate ZNF514 expression across different tumor types (Fig. 1A) and it was revealed that ZNF514 was commonly upregulated in various types of cancer, including EC, bladder urothelial carcinoma, cholangiocarcinoma and colon adenocarcinoma. Additionally, a quantitative comparison of ZNF514 expression using $\text{Log}_2(\text{TPM}+1)$ normalization across EC samples and matched healthy tissue revealed that ZNF514 was upregulated in most EC samples vs. healthy tissues (Fig. 1B). Additionally, the cBioPortal database was utilized to analyze the alteration types and frequencies of ZNF514 in EC from two different data sources from TCGA database (Nature 2017/Firehose Legacy). The analysis revealed that, among the 541 patients in the Nature 2017 data source, 8 patients had mutations (1.48%), 4 patients had amplifications (0.74%) and the gene alteration frequency was 2.22% (Fig. 1C). Among 185 patients in the Firehose legacy dataset, 0 patients had mutations (0%), while two patients had amplifications

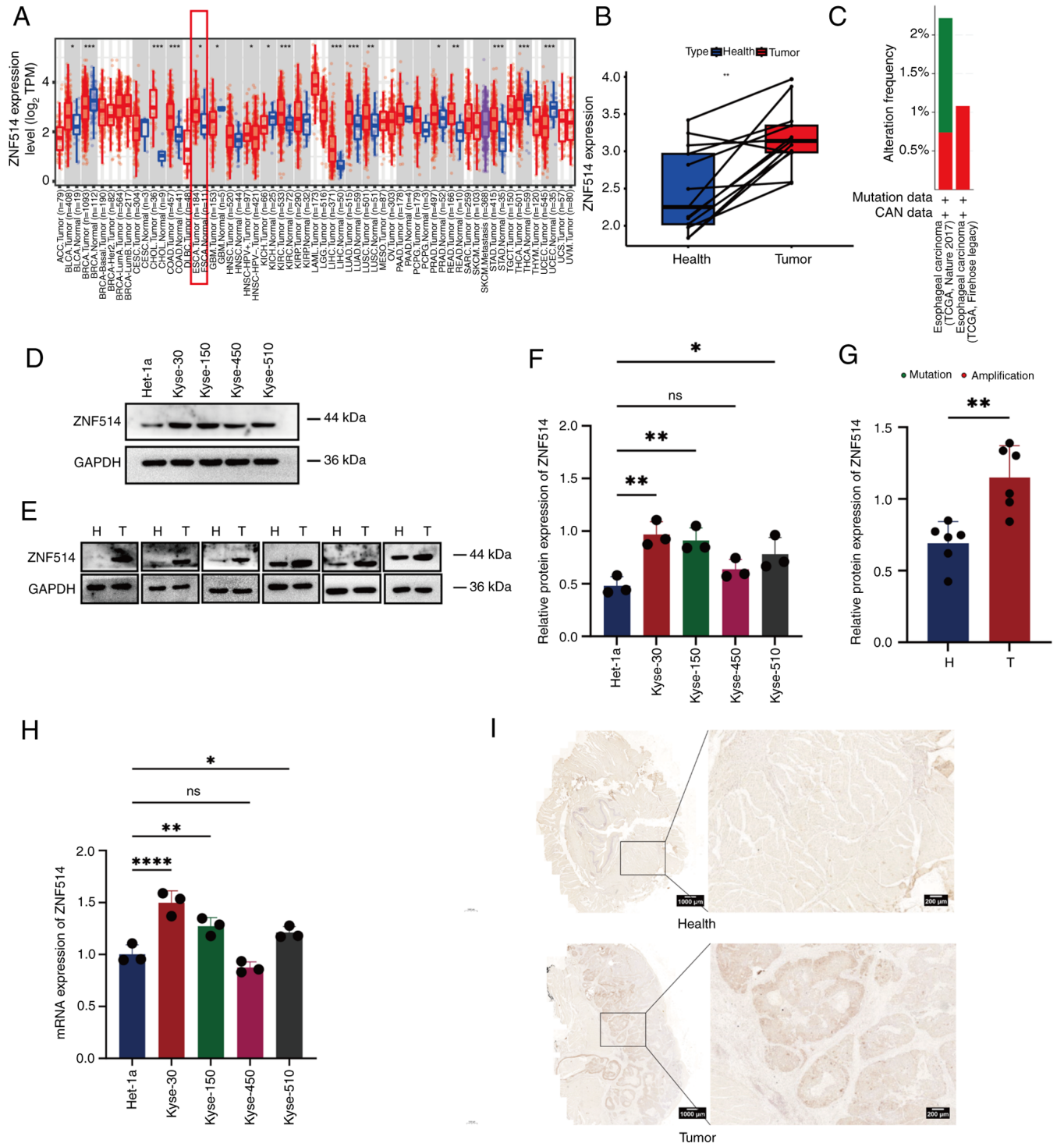

Figure 1. ZNF514 is significantly upregulated in EC tissues and cells. (A) Analysis of RNA expression differences of ZNF514 in normal and cancer tissues across various types of cancer using the Tumor Immune Estimation Resource database. (B) RNA expression differences between H and paired cancer tissues in patients with EC. (C) Gene alteration frequency of ZNF514 in EC. (D) Western blot analysis of ZNF514 protein expression differences in Het-1a and EC cell lines. (E) Western blot analysis of ZNF514 protein expression differences in the tumors and adjacent tissues of patients with EC. Semi-quantitative analyses of ZNF514 protein expression in (F) Het-1a and EC cell lines, and (G) tumor and adjacent tissues of patients with EC normalized to GAPDH. (H) Reverse transcription-quantitative PCR analysis of ZNF514 expression levels in Het-1a and EC cell lines. (I) Representative images of immunohistochemical staining for ZNF514 in the tumors and adjacent tissues of patients with EC . Scale bar, 1000 μm. *P<0.05, **P<0.01, ***P<0.001 and ****P<0.0001. H, Healthy; T, tumor; ZNF514, zinc finger protein 514; EC, esophageal cancer; ns, not significant; CNA, copy number alteration; TCGA, The Cancer Genome Atlas.

(1.08%), and the gene alteration frequency was 1.08% (Fig. 1C). Subsequently, RT-qPCR and western blotting were employed to examine the mRNA and protein expression levels of ZNF514 in Het-1a and multiple EC cell lines (Kyse-30, Kyse-150, Kyse-450 and Kyse-510). The results demonstrated that, with the exception of Kyse-450, both the protein (Fig. 1D and F) and mRNA expression levels (Fig. 1H) of ZNF514 were significantly elevated in these EC cell lines compared with those in the Het-1a cell line. To further assess the expression of ZNF514 in tissues, surgically resected EC tissues and adjacent

healthy tissues were collected and analyzed through western blotting (Fig. 1E and G) and IHC (Fig. 1I). The results showed that ZNF514 expression levels were higher in EC tissues than those in adjacent healthy tissues. These findings suggested that ZNF514 was upregulated in EC tissues and cells, indicating a close relationship between ZNF514 and the development and progression of EC.

Silencing ZNF514 leads to suppression of EC cell migration, invasion and proliferation. To investigate the functional role of ZNF514 in EC progression, phenotypic assays were performed following ZNF514 knockdown in Kyse-150 cells. First, the transfection efficiency of three ZNF514-specific siRNAs (siZNF514-1, siZNF514-2 and siZNF514-3) was validated using RT-qPCR (Fig. 2A) and western blotting (Fig. 2B and C). Based on these results, siZNF514-2 and siZNF514-3 were selected for subsequent functional analyses. Transwell migration and invasion assays (Fig. 2D-F), wound healing assay (Fig. 2G and H), colony formation assay (Fig. 2I and J), CCK-8 proliferation assay (Fig. 2K) and EdU assay (Fig. 2L and M) collectively showed that compared with the si-NT group, ZNF514 knockdown significantly inhibited migration, invasion and proliferation in EC cells. These findings indicated that silencing ZNF514 exerted a tumor-suppressive effect by restricting the migratory, invasive and proliferative capacities of EC cells.

Overexpression of ZNF514 increases migration, invasion and proliferation of EC cells. To explore the oncogenic role of ZNF514 in EC, phenotypic analyses were conducted following ZNF514 overexpression in Kyse-510 cells. First, the transfection efficiency of the ZNF514 overexpression plasmid was validated using RT-qPCR (Fig. 3A) and western blotting (Fig. 3B and C). Cells with stable overexpression then underwent functional assays. Transwell migration and invasion assays (Fig. 3D-F), wound healing assay (Fig. 3G and H), colony formation assay (Fig. 3I and J), CCK-8 proliferation assay (Fig. 3K) and EdU assay (Fig. 3L and M) revealed that ZNF514-overexpressing EC cells exhibited significantly enhanced migration, invasion and proliferative capacity compared with control EC cells transfected with empty vector plasmids. These results indicated that ZNF514 may act as an oncogene to facilitate EC progression by enhancing tumor cell motility and proliferative potential.

RNA-seq analysis following ZNF514 knockdown in Kyse-150 cells. Building on the previous findings, RNA-seq was performed on ZNF514-knockdown Kyse-150 150 EC s to explore the molecular mechanisms underlying ZNF514-mediated promotion of EC tumorigenesis and progression. Genes displaying significant expression level changes across various experimental conditions were termed DEGs. Significant DEGs were identified using the 'edgeR' software, with selection criteria including a $q<0.05$, fold-change >2 or $|\log_2(\text{fold-change})|>1$). This filtering process resulted in the identification of 1,901 DEGs, which included 260 upregulated genes and 1,641 downregulated genes (Fig. 4A and B). Subsequently, Pearson correlation analysis was performed on the identified DEGs. The Pearson correlation coefficient was 0.955, indicating an extremely strong positive correlation between the gene expression profiles of the si-NT group and the si-ZNF514 group. In terms of DEGs, red dots represent up-regulated genes, blue dots represent down-regulated genes, and gray dots represent genes with no significant differential expression. $P<2.2x10^{-16}$ (Fig. 4C). To further clarify the functional enrichment of DEGs, GO enrichment analysis categorized the DEGs into three primary categories: Biological processes, cellular components and molecular functions (Fig. 4D). The analysis indicated that these DEGs were significantly associated with molecular functions, including 'histone demethylase activity (H4-K20 specific)' and 'hedgehog receptor activity'. (Fig. 4E) Additionally, they were associated with biological processes such as 'histone H4-K20 demethylation' and 'positive regulation of acrosome reaction'.

KEGG pathway analysis was performed to identify key signaling pathways associated with the DEGs, aiming to clarify the mechanisms through which these genes impact cancer initiation and progression. The findings indicated that DEGs exhibited enrichment in pathways categorized into: Cellular Processes, including 'Cellular community', 'Cell growth and death' and 'Transport and catabolism'; Environmental Information Processing, including 'Signaling molecules and interaction', 'Membrane transport' and 'Signal transduction'; Genetic Information Processing including 'Transcription', 'Replication and repair', 'folding, sorting and degradation' and 'Translation'; Human Diseases, including 'Infectious diseases: Viral', 'Cancers: Specific types' and 'Immune diseases'; Metabolism, including 'Energy metabolism' and 'Nucleotide metabolism'; and Organismal Systems, including 'Immune system' and 'Digestive system' (Fig. 4F). The bubble plot illustrated that DEGs were significantly enriched in pathways related to 'Complement and coagulation cascades', 'Alcoholism', 'Pertussis', 'Systemic lupus erythematosus' and 'Transcriptional misregulation in cancer' (Fig. 4G). The STRING database was used for PPI analysis and to build a PPI network of DEGs. The resulting comprehensive overview revealed that the ZNF514-related protein network primarily consisted of histone families, which were structural constituents of chromatin, and associated troponins of the troponin complex, including histones H2A, H2B, H3 and the troponin proteins TNNC1, TNNC2, TNNT2 and NKX2-5 (Fig. 4H).

GSEA of the RNA-seq. GSEA was carried out on the DEGs obtained through RNA-seq analysis. The enrichment score (ES) was calculated and normalized to produce the normalized ES (NES), thereby standardizing the gene set data. By calculating the ES and evaluating its significance, enrichment plots for various pathways were generated. In the analysis results, the criteria of $P<0.05$, $|NES|>1$ and q-value <0.25 were regarded as significantly enriched. GSEA revealed that the Fcγ receptor (FCGR)-dependent phagocytosis (Fig. 5A), FCGR activation (Fig. 5B) and the initial triggering of complement (Fig. 5C) were activated. Additionally, G-protein coupled receptor (GPCR) ligand binding (Fig. 5D), G-protein βγ (Gβγ) signaling through PI3Kγ (Fig. 5E) and ribosomal S6 kinase (RSK) activation (Fig. 5F) were inhibited. These results suggested that ZNF514 regulation may affect EC immunosurveillance via FCGR-dependent phagocytosis, FCGR activation, and initial complement triggering; it may also influence EC occurrence

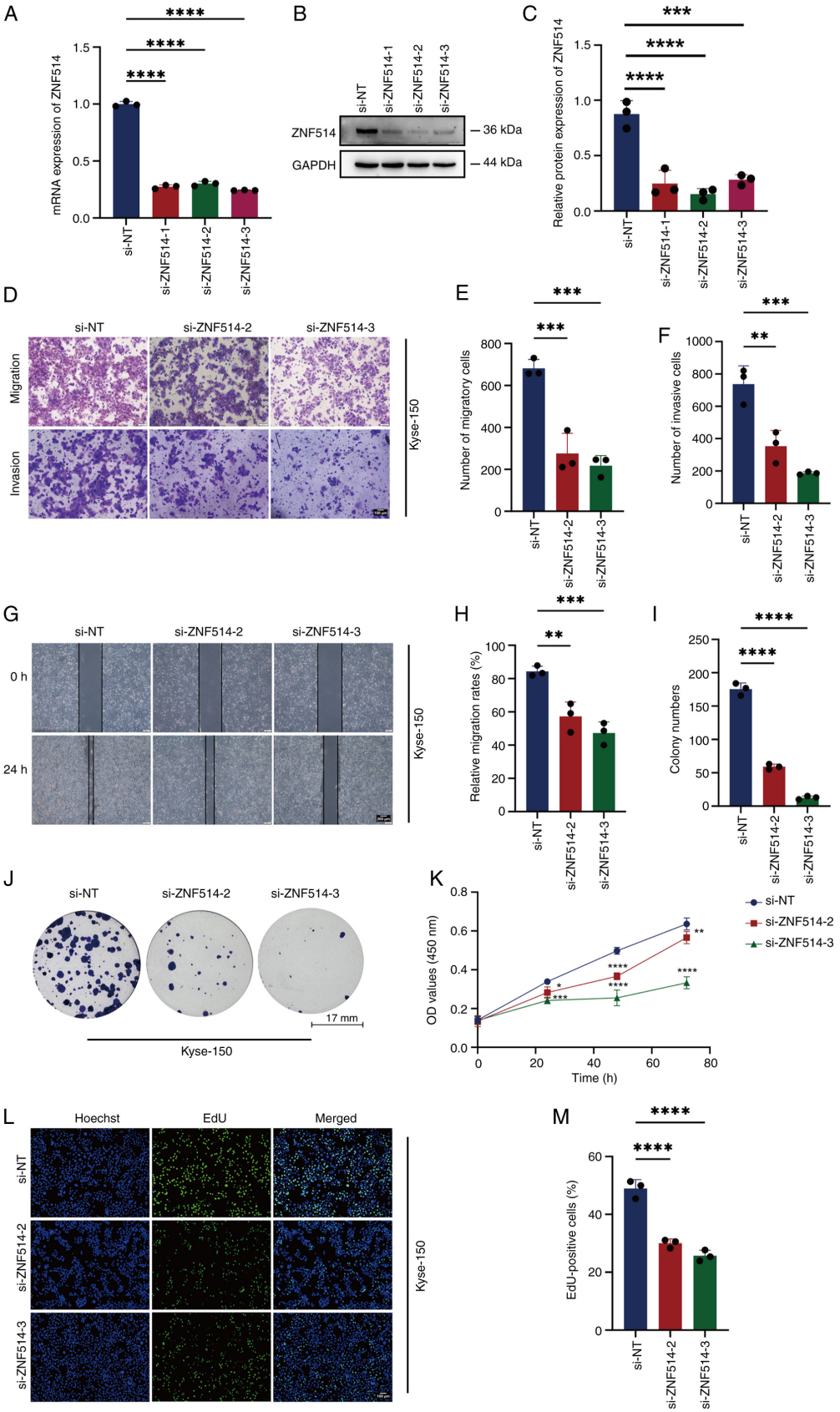

Figure 2. Downregulation of ZNF514 inhibits proliferation, migration and invasion of Kyse-150 cells. ZNF514 mRNA and protein expression levels in Kyse-150 cells transfected with targeted siRNAs were analyzed using (A) reverse transcription-quantitative PCR and (B) western blot analysis, alongside (C) semi-quantitative analysis of ZNF514 protein levels. (D) Effects of ZNF514 knockdown on the migration and invasion of Kyse-150 cells was assessed using Transwell assays; (E) quantitative analysis of the migration assay, (F) quantitative analysis of the invasion assay. Scale bar, 100 μm. (G) Wound healing assays were conducted to evaluate the effect of ZNF514 knockdown on the migration of Kyse-150 cells; (H) quantitative analysis of cell migration rate. Scale bar, 200 μm. (I) Quantitative analysis of colony formation, (J) colony formation, (K) Cell Counting Kit -8, (L) EdU assays, and (M) quantitative analysis of the EdU assay were utilized to evaluate the effects of ZNF514 knockdown on the proliferation of Kyse-150 cells. Scale bar, 100 μm. *P<0.05, **P<0.01, ***P<0.001 and ****P<0.0001 vs. si-NT. NT, non-targeting; ZNF514, zinc finger protein 514; CCK-8, Cell Counting Kit-8; si, small interfering; EdU, 5-ethynyl-2'-deoxyuridine.

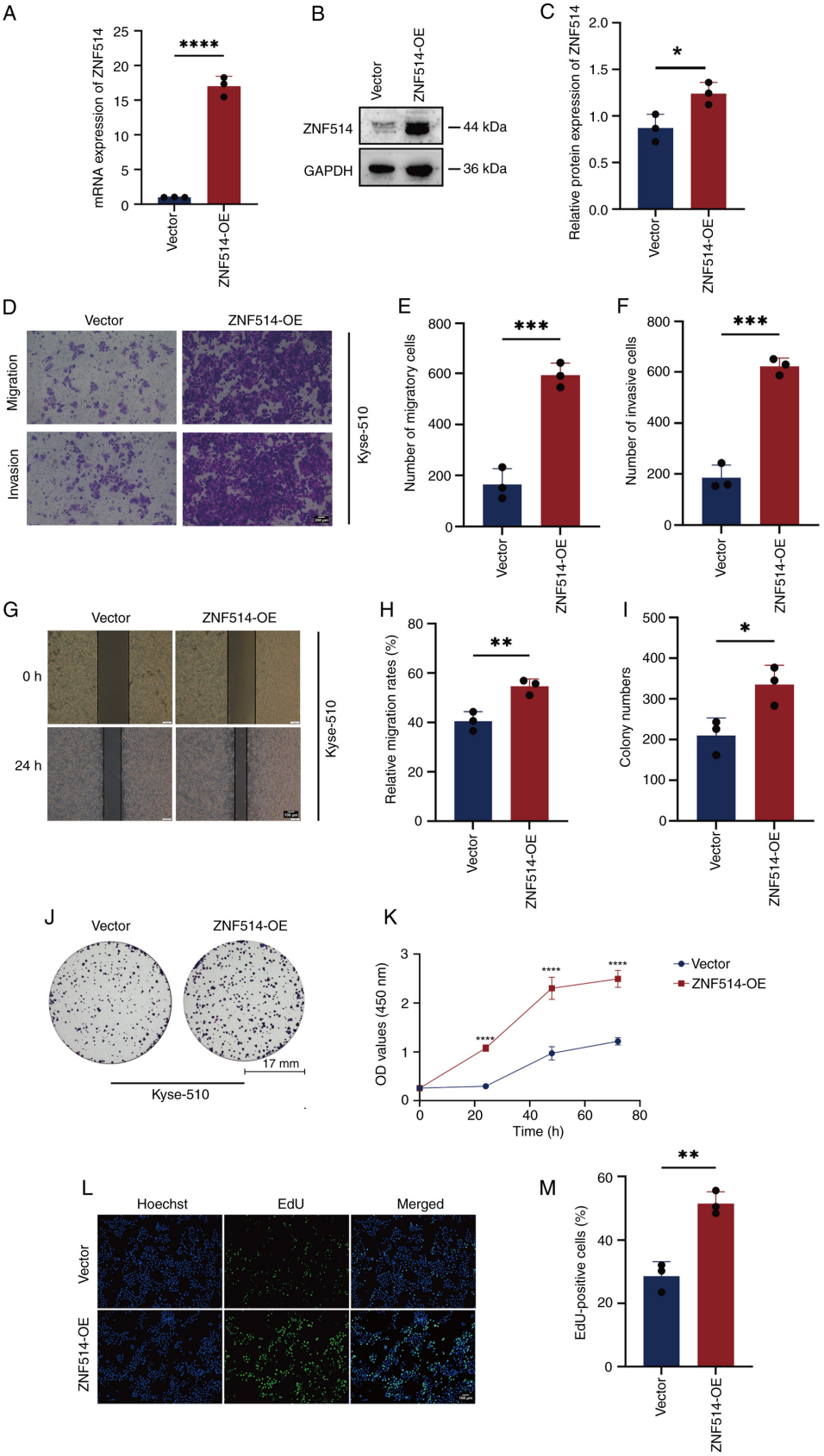

Figure 3. OE of ZNF514 promotes proliferation, migration and invasion of Kyse-510 cells. Analysis of ZNF514 mRNA and protein expression in Kyse-510 cells transfected with targeted OE plasmid using (A) reverse transcription-quantitative PCR and (B) western blot analysis, along with (C) semi-quantification of ZNF514 protein. (D) Transwell assays were performed to evaluate the effects of ZNF514 OE on the migration and invasion of Kyse-510 cells; (E) quantitative analysis of the migration assay, (F) quantitative analysis of the invasion assay. Scale bar, 200 μm. (G) Wound healing assays were conducted to assess the impact of ZNF514 OE on the migration of Kyse-510 cells. (H) quantitative analysis of cell migration rate. Scale bar, 100 μm. (I) Quantitative analysis of colony formation, (J) Colony formation, (K) Cell Counting Kit-8, (L) EdU assays, and (M) quantitative analysis of the EdU assay were utilized to evaluate the effects of ZNF514 OE on the proliferation of Kyse-510 cells. Scale bar, 100 μm. *P<0.05, **P<0.01, ***P<0.001 and ****P<0.0001 vs. vector. ZNF514, zinc finger protein 514; OE, overexpression; EdU, 5-ethynyl-2'-deoxyuridine.

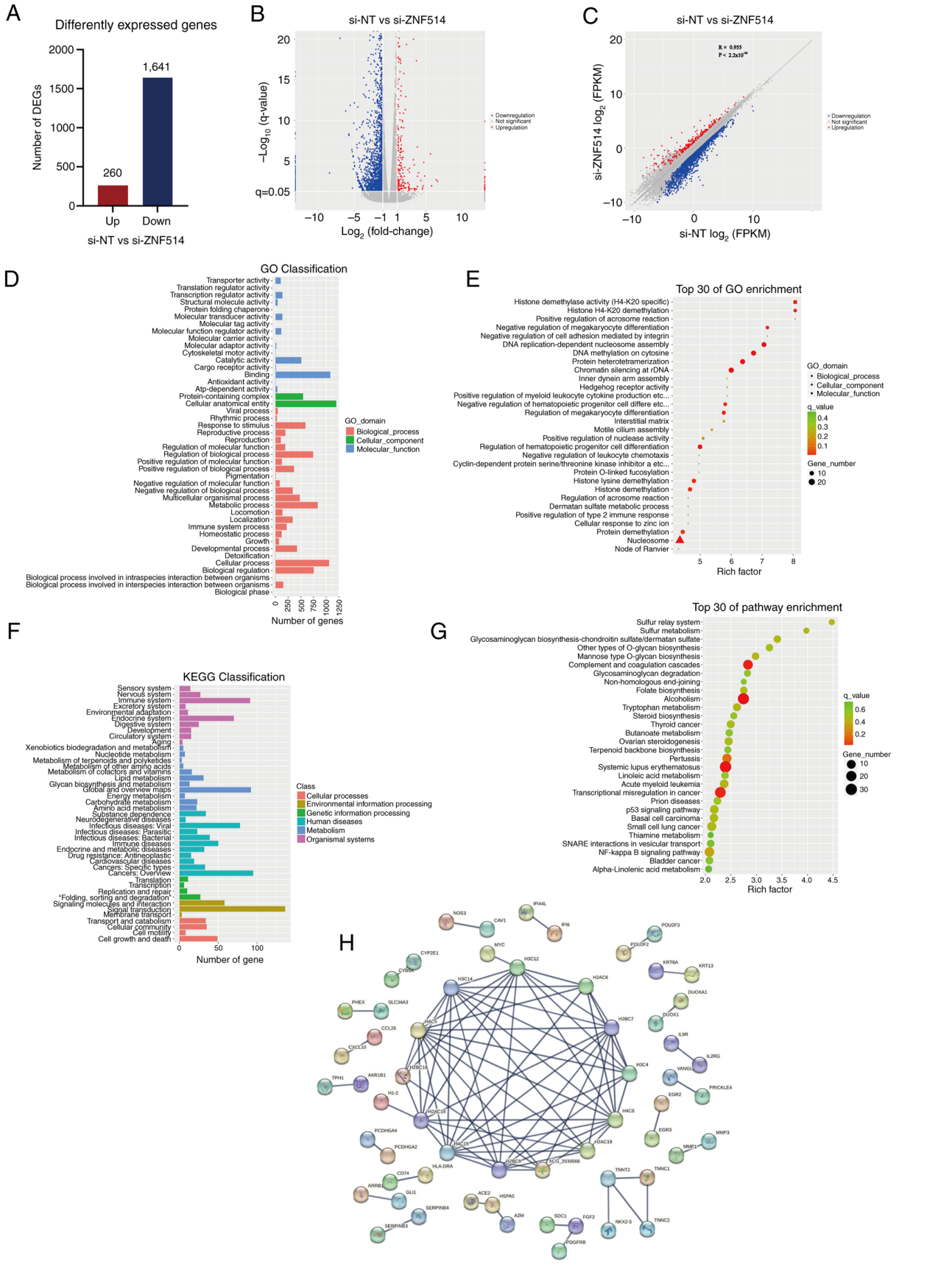

Figure 4. RNA sequencing analysis of esophageal cancer cells reveals the mechanisms by which downregulation of ZNF514 contributes to cancer progression. (A) Bar graph displaying the number of genes affected by ZNF514 knockdown, selected based on the criteria of $|\log_2(\text{Fold-change})|>1$ and q-value <0.05. (B) Volcano plot illustrating the expression of DEGs, with red indicating upregulated genes and blue signifying downregulated genes. (C) Scatter plot showing the correlation of DEGs, with red indicating upregulated genes and blue signifying downregulated genes. (D) GO functional classification of DEGs, (E) GO enrichment analysis of DEGs, (F) KEGG pathway classification of DEGs, and (G) KEGG pathway enrichment analysis of DEGs. (H) Protein-protein interaction analysis was conducted based on the DEGs. DEG, differentially expressed gene; ZNF514, zinc finger protein 514; GO, Gene Ontology; KEGG, Kyoto Encyclopedia of Genes and Genomes; si-NT, siRNA-non-targeting.

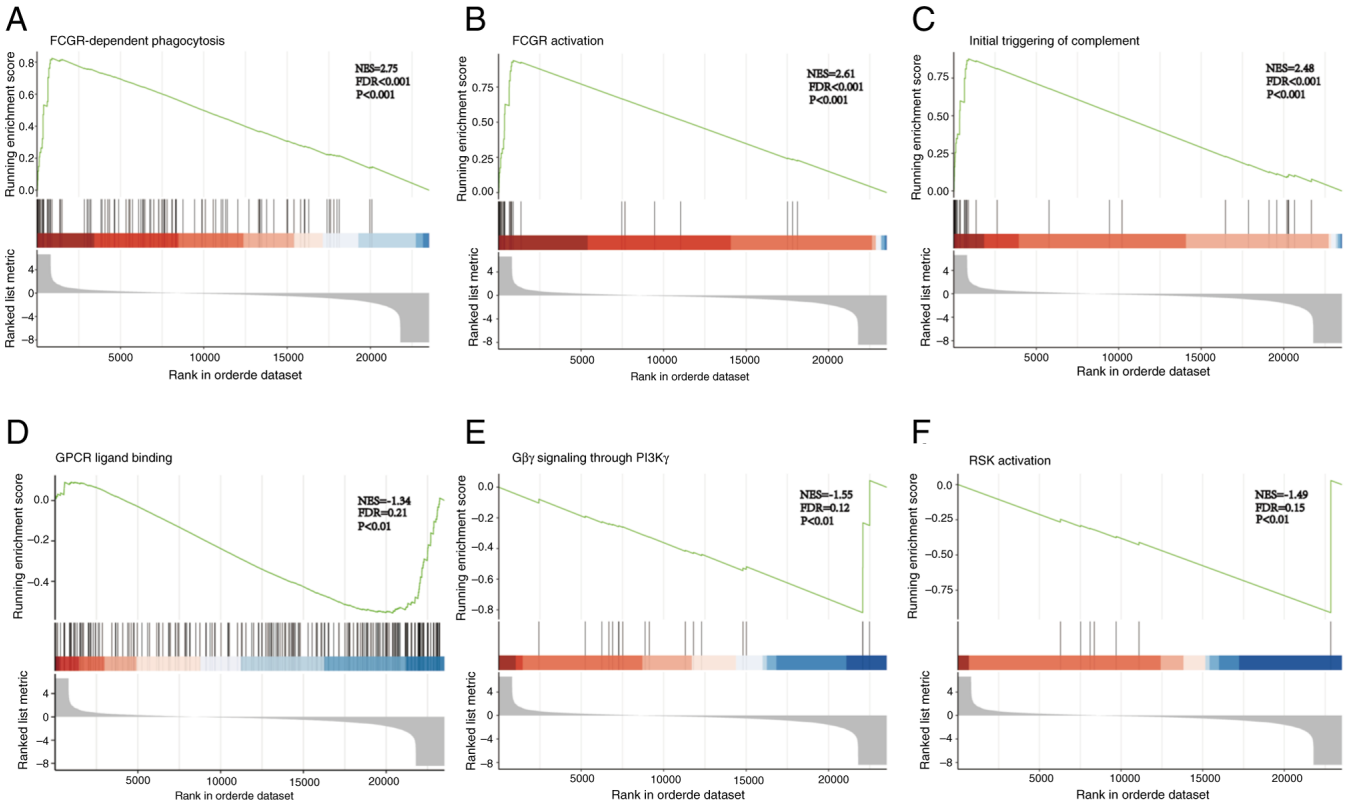

Figure 5. GSEA of differentially expressed genes. The enrichment plots demonstrated that (A) FCGR-dependent phagocytosis, (B) FCGR activation and (C) initial triggering of complement were activated, whereas (D) GPCR ligand binding, (E) Gβγ signaling through PI3Kγ and (F) RSK activation were inhibited; FCGR, Fcγ receptor; GPCR, G-protein coupled receptor; RSK, ribosomal S6 kinase.

and development by regulating oncogenic signaling cascades through GPCR ligand binding, Gβγ signaling via PI3Kγ, and RSK activation.

IPA of the DEGs identified by RNA-seq analysis uncovers their potential mechanisms of influence on EC progression. To investigate the mechanism by which ZNF514 influences EC progression, IPA of the DEGs was performed. After ZNF514 knockdown in Kyse-150 cells, significantly upregulated genes included A2M, CTC_435M103, IGHG1, IGHA1, RP11_140H171, TGFB2-OT1, BCL2A1, POSTN, RP11-235E17.2 and IGFBP5 (Fig. 6A). Conversely, the significantly downregulated genes included ATP6V1G2-DDX39B, LINC02474, H3C12, KRT33B, CLDN16, AP0008926, RP11_327E25, SLAMF7, CTD_2349B81 and MMP1 (Fig. 6B). Enrichment analysis indicated that these genes were significantly associated with multiple pathologies, such as 'Failure of kidney', 'Renal impairment', 'Retinal dystrophy', 'Macular dystrophy or cone-rod dystrophy', 'Genitourinary carcinoma' and 'Abdominal aortic aneurysm'. (Fig. 6C).

Pathway enrichment analysis identified several significantly affected pathways (negative Z-score indicates that the pathway is significantly inhibited, while a positive Z-score indicates the pathway is significantly activated.), encompassing the 'Atherosclerosis Signaling' pathway, 'Hematoma Resolution Signaling Pathway', 'Regulation of the Epithelial Mesenchymal Transition by Growth Factors Pathway', 'NOD1/2 Signaling Pathway', 'Molecular Mechanisms of Cancer', 'IL-17 Signaling' pathway and 'CGAS-STING Signaling Pathway'. Based on the Z-value results, including the following pathways were significantly inhibited: 'Molecular Mechanisms of Cancer'; 'Regulation of the Epithelial Mesenchymal Transition by Growth Factors Pathway'; 'NOD1/2 Signaling Pathway' and 'IL-17 Signaling Pathway' (Fig. 6D). The present study found that 'Molecular Mechanisms of Cancer' was the pathway with the furthest Z-score from 0 (-4.323), indicating that the pathway was subjected to the most significant inhibition. Subsequent analysis of the pathways within 'Molecular Mechanisms of Cancer' revealed that the PI3K/AKT pathway was widely inhibited (Fig. 7A). Therefore, it was highly plausible that the low expression of ZNF514 exerted its effects on cellular biological functions by suppressing the upstream PI3K/AKT pathway, which in turn would lead to the inhibition of multiple downstream pathways. The 'Regulation of the Epithelial Mesenchymal Transition by Growth Factors Pathway' was implicated in epithelial-mesenchymal transition (EMT) regulation, with multiple pathways, such as the Ras/MEK and PI3K/AKT pathways, found to be inhibited following ZNF514 knockdown. Fig. S1 illustrates the key molecules involved in these pathways. Furthermore, the related molecules in the 'STAT3 pathway' (Fig. S2) and 'NOD1/2 Signaling Pathway' (Fig. S3) were significantly inhibited. Additionally, the related molecules of NF-κB in the 'Molecular Mechanisms of Cancer' were significantly inhibited. The upstream factors of ZNF514 were also identified, with TBX3 (Fig. 7B), and TLR5 (Fig. 7C) being recognized as significant upstream regulators. Notably, TBX3 was significantly activated, while TLR5 was significantly inhibited.

A

Molecules	Expr. Value
A2M	↑ 6.614
CTC_435M103	↑ 6.427
IGHG1	↑ 5.803
IGHA1	↑ 5.781
RP11_140H171	↑ 5.642
TGFB2-OT1	↑ 4.830
BCL2A1	↑ 4.702
POSTN	↑ 4.690
RP11-235E17.2	↑ 4.616
IGFBP5	↑ 4.521

B

Molecules	Expr. Value
ATP6V1G2-DDX39B	↓ −8.413
LINC02474	↓ −6.966
H3C12	↓ −6.162
KRT33B	↓ −5.725
CLDN16	↓ −5.705
AP0008926	↓ −5.544
RP11_327E25	↓ −5.308
SLAMF7	↓ −5.257
CTD_2349B81	↓ −5.220
MMP1	↓ −5.203

C

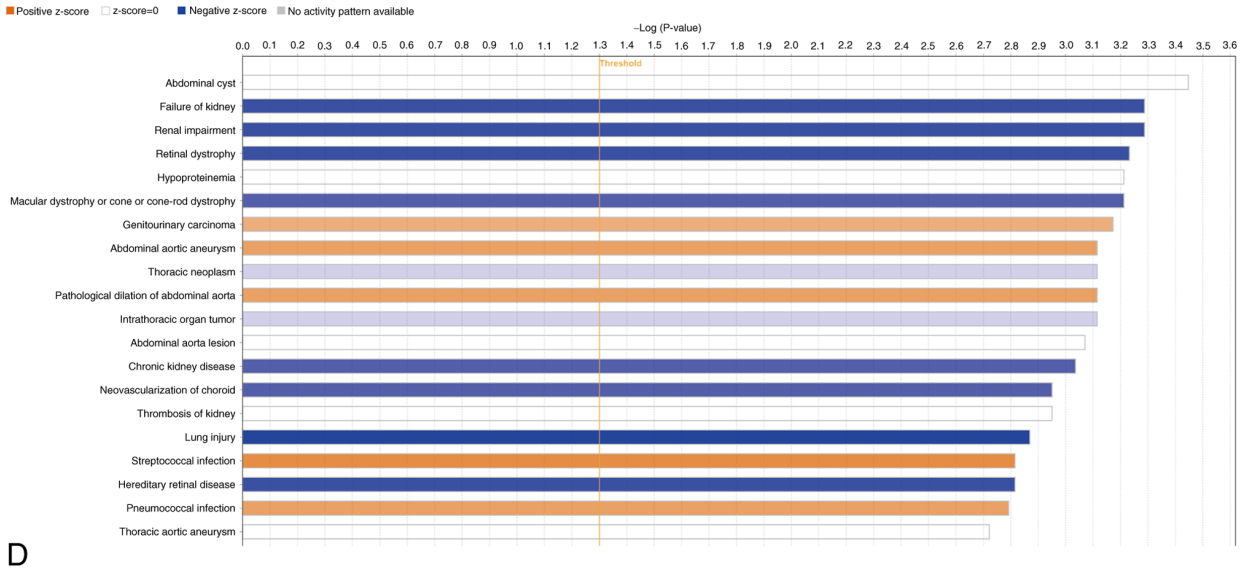

D

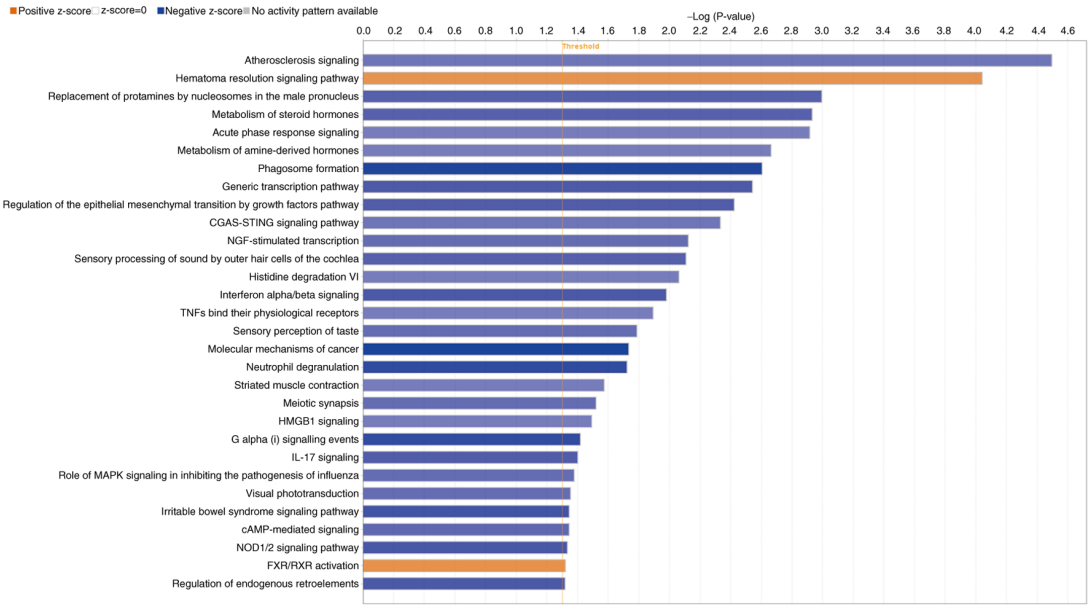

Figure 6. Ingenuity Pathway Analysis of DEGs from RNA sequencing analysis. The top 10 significantly (A) upregulated and (B) downregulated genes following ZNF514 knockdown in Kyse-150 cells, based on $\log_2$(Fold-change). (C) Enrichment analysis of disease-related genes. (D) Pathway enrichment analysis based on DEGs. The pathways are indicated in orange for significant activation and blue for significant inhibition, based on z-score analysis. DEG, differentially expressed gene; ZNF514, zinc finger protein 514.

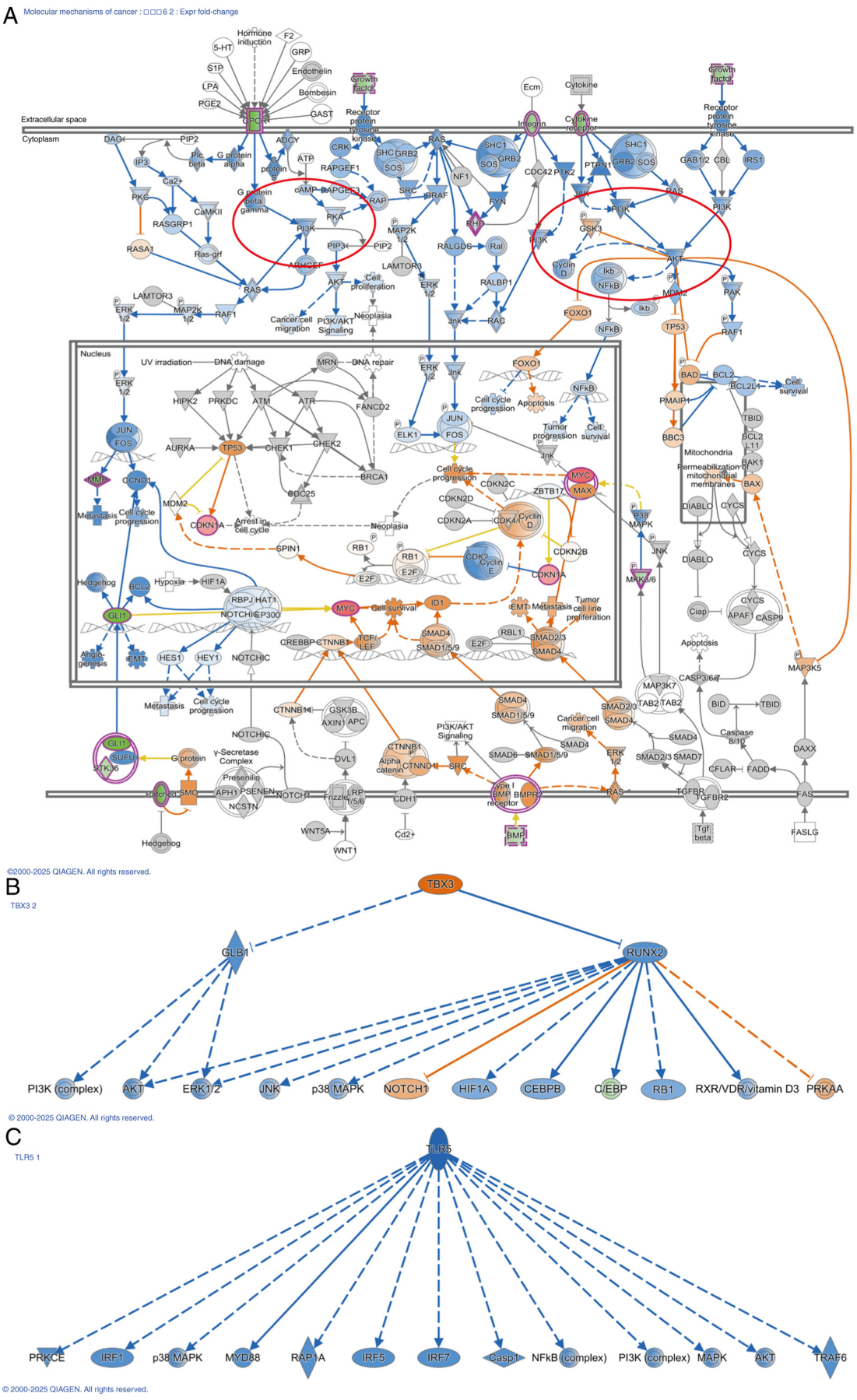

Figure 7. IPA shows that ZNF514 knockdown affects multiple cancer-related pathways. (A) The affected PI3K/AKT pathway, and its upstream and downstream relationships in the Molecular Mechanisms in Cancer pathway. (B) Activation of TBX3, and (C) inhibition of TLR5, with the downstream molecules influenced by these factors shown. Solid line, direct interaction; dashed line, indirect interaction. Arrow, activation; Blocked arrow, inhibition. Blue, leads to inhibition; Orange, leads to activation; Yellow, findings inconsistent with state of downstream molecule; Gray, effect not predicted.

In conclusion, the present findings suggested that the antitumor mechanisms of ZNF514 downregulation might be linked to the suppression of the PI3K/AKT and Ras/MEK pathways, as well as the STAT3 pathway, nucleotide oligomerization domain receptor (NOD)1/2 pathway and NF-κB pathway. Therefore, low expression of ZNF514 may suppress EC progression by inhibiting these classical oncogenic pathways, making ZNF514 a notable target for EC treatment.

Discussion

ZNFs, defined by their conserved zinc finger motifs, represent one of the largest families of transcription factors in the human genome and are important in a number of diverse biological processes, such as differentiation, cell development, metabolic regulation and apoptosis (14). The C2H2 is the largest class among all zinc finger types, comprising the sequence CX2CX3FX5LX2HX3H. Upon interaction with zinc ions, the two cysteine and two histidine residues fold into a finger-like structure comprising an α-helix and a double-stranded anti-parallel β-sheet (5). Each C2H2-type ZNF typically contains KRAB, BTB, SCAN and SET domains, and multiple zinc finger motifs capable of binding to DNA sequences. ZNF514, a member of the KRAB-type C2H2 ZNF family, encompasses two core domains: The N-terminal KRAB domain (residues 74-111), which acts as a key transcriptional repressor by recruiting corepressors such as KRAB-associated protein 1 to modulate chromatin states and facilitate epigenetic regulation; and seven C2H2 zinc finger domains at the C-terminus (residues 307-400), each featuring a conserved Cys2/His2 motif that enables sequence-specific DNA binding and thereby mediates the regulation of gene promoter regions, underpinning its function as a transcription factor (15-17).

Studies have shown that ZNF family can perform distinct functions with various partners, potentially leading to antagonistic interactions with different partners. For example, zinc finger E-box-binding homeobox 1 is a transcriptional repressor closely associated with cell differentiation genes, which can interact with yes-associated protein 1 to promote the invasive phenotype of cancer (18). ZNF family exhibit diverse regulatory mechanisms for various downstream genes by recruiting different chromatin modifiers. For example, ZNF217 modifies downstream genes by interacting with REST corepressor 1, lysine demethylase 1, histone deacetylase 2 and C-terminal binding protein, thereby influencing their expression (19).

Additionally, post-translational modifications of ZNF family provide another layer of regulation. Phosphorylation of serine or threonine residues on ZNF-linked peptides has previously been reported. During mitosis, ZNFs such as Ikaros, Sp1 and YY1 exhibit high levels of phosphorylation on threonine/serine residues in the linked peptides of ZNF family, leading to a loss of DNA-binding ability (5). Furthermore, research has indicated that ZNFs can affect tumor cell migration and invasion by regulating the EMT process. The A20 protein belongs to the Cys2/Cys2 ZNF family (20), where it induces the monoubiquitination of Snail1 at three lysine residues, thereby decreasing its phosphorylation. Consequently, the monoubiquitinated Snail1 is stabilized in the nucleus and promotes EMT and basal-like breast cancer metastasis induced by transforming growth factor-β1 (21). Multiple ZNFs have emerged as potential biomarkers and effective therapeutic targets in cancer (22-24). However, research on ZNF514 in EC is limited and the mechanisms by which it functions in EC remain to be elucidated.

In the present study, ZNF514 exhibited significant upregulation in EC tissues. Furthermore, functional assays, such as siRNA-mediated knockdown experiments, supported the role of ZNF514 in promoting EC cell migration, invasion and proliferation. Mechanistically, ZNF514 inhibition may suppress tumorigenesis by disrupting multiple oncogenic pathways, including PI3K/AKT, Ras/MEK, STAT3, NOD1/2 and NF-κB signaling cascades. Collectively, the findings of the present study established ZNF514 as a central regulator of EC progression, highlighting its potential as a therapeutic target and prognostic biomarker.

In the present study, RNA-seq analysis of Kyse-150 cells after ZNF514 knockdown, followed by GO and KEGG analyses, GSEA and IPA of the transcriptomics data, indicated that ZNF514 modulated multiple signaling pathways, functioning as an upstream regulator and consequently impacting EC progression. GSEA further revealed that ZNF514 knockdown in Kyse-150 cells activated FCGR-dependent phagocytosis, increased FCGR activation and promoted early complement triggering compared with normal Kyse-150 cells. Additionally, GPCR ligand binding, Gβγ signaling via PI3Kγ and RSK activation were significantly inhibited. Meanwhile, IPA corroborated the reliability of the GSEA findings, showing that the Ras/MEK, PI3K/AKT, STAT3, NOD1/2 and NF-κB pathways were inhibited in the transcriptome following ZNF514 knockdown.

FCGRs are a family of transmembrane glycoproteins that exert anti-pathogen effects by specifically binding to the Fc region of IgG antibodies. These receptors are expressed across diverse immune cell types, establishing a robust defense mechanism to eliminate invading pathogens (25). Studies have shown that the bispecific antibody MDX-H210 can target FCGR1 (FcγRI) on cytotoxic effector cells with upregulated FcγRI expression, thereby activating these effector cells to target HER2/neu-overexpressing malignancies (26).

The complement system is part of the innate immune system and protects the host against pathogen invasion after activation via the classical, alternative and lectin pathways (27). The complement system exerts dual effects on cancer progression. Furthermore, the interactions of complement components are specific to each cancer type, and are regulated by tumor cell characteristics and the tumor microenvironment (28). The effects of the complement system on malignancies are determined by a combination of complement-mediated antitumor and cytotoxicity, along with C5a/C5aR1 axis-mediated protumor chronic inflammation that hinders antitumor T-cell responses (29). Although the mechanisms by which complement system activation via ZNF514 downregulation affects tumor cells are yet to be elucidated, the increase in cytotoxic effects resulting from FCGR activation suggests that the activation of the complement system in the present study may have enhanced immune cell toxicity, thereby inhibiting tumor progression. Therefore, ZNF514 downregulation may have promoted the activation of FCGRs and the complement system, thereby enhancing cytotoxic effects to kill tumor cells.

GPCRs, which constitute ~4% of the human genome, represent the largest family of cell surface receptors. These receptors mediate cell communication by transducing external signals into internal cellular responses (30). By binding to ligands, they activate various Gα proteins, including Gαs, Gαi, Gαq and Gα12/13, subsequently triggering downstream signaling cascades. These signaling cascades regulate cell migration, transcription, proliferation and survival via kinases and phosphatases, including MAPK, AKT and mTOR (31). This indicates that GPCR activation is closely associated with cancer initiation and progression.

An important step in neutrophil chemotaxis involves the transformation of PIP2 into PIP3 by PI3Kγ, which is also important for the metastasis of multiple cancer types (32). The Gβγ heterodimer can recruit PI3Kγ to the cell membrane and activate the kinase activity of PI3Kγ via allosteric regulation, enabling PI3Kγ to convert PIP2 into PIP3. This activates the PI3K signaling pathway and subsequently triggers pro-tumorigenic signaling cascades (32). RSK is a signaling molecule located downstream of the Ras/MAPK signaling pathway and its activation promotes cellular biological functions such as proliferation, growth, motility and survival (33). Thus, downregulation of 'Gβγ signaling through the PI3Kγ' and RSK pathways may inhibit tumor progression, a finding that the present study emphasizes.

Furthermore, transcriptomic IPA revealed that the tumor-suppressive mechanisms associated with ZNF514 downregulation may involve inhibition of the Ras/MEK, PI3K/AKT, STAT3, NOD1/2 and NF-κB pathways. EGF is important in governing cell growth, proliferation and differentiation. Additionally, it is linked to cancer stemness and EMT (34), with the Ras/Raf/MAPK pathway considered a traditional downstream signaling pathway of EGF/EGF receptor interactions. The Ras-ERK signaling cascade is activated by growth factors that bind to receptor tyrosine kinases (35,36), leading to the activation of the small G-protein Ras. Subsequently, MEK, RAF and ERK are activated sequentially in a phosphorylation-dependent cascade, with ERK1/2 ultimately phosphorylating downstream effectors which regulate numerous physiological processes, including proliferation, transcription, survival, cell adhesion, growth and differentiation (35,37,38). Aberrant activation of the PI3K/AKT/mTOR pathway markedly contributes to carcinogenesis by driving cancer initiation and progression via its impact on cell proliferation (39,40), autophagy (41,42), apoptosis (43), angiogenesis (44,45) and EMT (46,47). Activation of STAT3 is closely associated with various epithelial (48), mesenchymal (49) and hematological tumors (50), and STAT3 activation is key for the malignant phenotype (51). Research indicates that STAT3 binds to the TWIST promoter to mediate its transcriptional upregulation, consequently triggering EMT (52).

NOD1 primarily participates in innate inflammatory immune responses by mediating the NF-κB, MAPK and autophagy-related pathways. Uncontrolled apoptosis regulated by NOD1 may induce an immunosuppressive microenvironment that facilitates tumor progression (53). By contrast, NOD2 is associated with chronic inflammation and cancer development (54). The NF-κB pathway has long been recognized as a prototypical pro-inflammatory signaling pathway that is frequently overactivated in tumors (55). Additionally, NF-κB activation is observed in cancer cells and the tumor microenvironment of most solid tumors and hematological malignancies. This activation contributes to genetic and epigenetic alterations, metabolic reprogramming, the acquisition of cancer stem cell traits, EMT, invasion, angiogenesis and metastasis (55).

Through bioinformatics analyses and *in vitro* cell experiments, the present study revealed the important role of ZNF514 in the progression of EC. ZNF514 may serve a notable role in regulating cell motility and the invasive potential of EC cells. The present study aimed to explore the role of high ZNF514 expression in the mechanism of EC progression using EC cell models and did not perform *in vivo* experiments. In future research, it is necessary to establish EC animal models, such as immunodeficient mouse xenograft models, and combine techniques, such as *in vivo* imaging and histopathological analysis, to further validate the pro-cancer effects and molecular pathways of ZNF514 in the *in vivo* environment, and to elaborate its role in driving EC initiation and progression. Meanwhile, the small sample size of the present study also constitutes a limitation. In the future, we aim to expand the sample size, conduct more comprehensive clinical validations, and further explore the relationship between ZNF514 expression and the prognosis of patients with EC. In addition, the lack of validation experiments based on RNA-seq and pathway analysis was also a limitation of the present study. The study of the mechanism of ZNF514 in EC remains in its initial stage and further experimental verification is needed. This validation will not only establish a solid foundation for the present conclusions but also provide a scientific rationale for developing ZNF514-targeted small-molecule compounds and their clinical translation.

The present study represents, to the best of our knowledge, the first report on the role of ZNF514 in EC, demonstrating that ZNF514 may be highly expressed in patients with EC. Its overexpression may drive the proliferation, motility and invasiveness of EC cells. The present study also revealed that ZNF514 can modulate the biological behavior of EC cells by engaging multiple signaling pathways. Its mechanism may predominantly regulate EC progression via the PI3K/AKT pathway, underscoring its multifunctional role. The findings of the present study merit further investigation into the specific molecular mechanisms underlying the diverse regulatory functions of ZNF514. Furthermore, the present study established a robust theoretical framework for exploring the specific mechanisms underlying the multifaceted function of ZNF514. This not only facilitates the development of targeted therapies across diverse cancer types, but also accelerates the advancement of EC diagnosis and treatment in clinical settings. Notably, the present study has laid an experimental foundation for the molecular functions of ZNF514 in EC.

Acknowledgements

Not applicable.

Funding

The present study was financially supported by the Shandong Province Medical and Health Development Plan (grant no. 202304020860) and the Jinan Municipal Health Commission Science and Technology Development Plan Project (grant no. 2024302003).

Availability of data and materials

The data generated in the present study may be requested from the corresponding author. The RNA sequencing data generated in the present study have been deposited in the Gene Expression Omnibus database under accession number GSE301311 or at the following URL: https://www.ncbi.nlm.nih.gov/geo/query/acc.cgi?acc=GSE301311.

Authors' contributions

LZ and HL conceived and designed the study. LL, GW and CZ conducted the experiments; LL, XS and HZ performed the bioinformatics analysis. LZ revised the manuscript. LZ and XS confirm the authenticity of all the raw data. All authors read and approved the manuscript.

Ethics approval and consent to participate

The present study was approved by the institutional review board of Jinan Central Hospital (approval no. 20241120027). All subjects provided written informed consent form before enrollment in the study.

Patient consent for publication

Patients provided written informed consent regarding publishing their data.

Competing interests

The authors declare that they have no competing interests.

Use of artificial intelligence tools

During the preparation of this work, the AI tool ChatGPT (https://chatgpt.com) was used to improve the readability and language of the manuscript, and subsequently, the authors revised and edited the content produced by the AI tools as necessary, taking full responsibility for the ultimate content of the present manuscript.

References

1. Deboever N, Jones CM, Yamashita K, Ajani JA and Hofstetter WL: Advances in diagnosis and management of cancer of the esophagus. BMJ 385: e074962, 2024.
2. Smyth EC, Lagergren J, Fitzgerald RC, Lordick F, Shah MA, Lagergren P and Cunningham D: Oesophageal cancer. Nat Rev Dis Primers 3: 17048, 2017.
3. Huang FL and Yu SJ: Esophageal cancer: Risk factors, genetic association, and treatment. Asian J Surg 41: 210-215, 2018.
4. Lin L and Lin DC: Biological significance of tumor heterogeneity in esophageal squamous cell carcinoma. Cancers (Basel) 11: 1156, 2019.
5. Jen J and Wang YC: Zinc finger proteins in cancer progression. J Biomed Sci 23: 53, 2016.
6. Hong K, Yang Q, Yin H, Wei N, Wang W and Yu B: Comprehensive analysis of ZNF family genes in prognosis, immunity, and treatment of esophageal cancer. BMC Cancer 23: 301, 2023.
7. Jen J, Lin LL, Lo FY, Chen HT, Liao SY, Tang YA, Su WC, Salgia R, Hsu CL, Huang HC, *et al*: Oncoprotein ZNF322A transcriptionally deregulates alpha-adducin, cyclin D1 and p53 to promote tumor growth and metastasis in lung cancer. Oncogene 36: 5219, 2017.
8. Yao J, Qian K, Chen C, Liu X, Yu D, Yan X, Liu T and Li S: Correction for: *ZNF139/circZNF139* promotes cell proliferation, migration and invasion via activation of PI3K/AKT pathway in bladder cancer. Aging (Albany NY) 14: 4927-4928, 2022.
9. Wang Y, Gong Y, Li X, Long W, Zhang J, Wu J and Dong Y: Targeting the ZNF-148/miR-335/SOD2 signaling cascade triggers oxidative stress-mediated pyroptosis and suppresses breast cancer progression. Cancer Med 12: 21308-21320, 2023.
10. Cancer Genome Atlas Research Network; Analysis Working Group: Asan University; BC Cancer Agency; Brigham and Women's Hospital; Broad Institute; Brown University; Case Western Reserve University; Dana-Farber Cancer Institute; Duke University; Greater Poland Cancer Centre, *et al*: Integrated genomic characterization of oesophageal carcinoma. Nature 541: 169-175, 2017.
11. Livak KJ and Schmittgen TD: Analysis of relative gene expression data using real-time quantitative PCR and the 2(-Delta Delta C(T)) method. Methods 25: 402-408, 2001.
12. Robinson MD, McCarthy DJ and Smyth GK: edgeR: A Bioconductor package for differential expression analysis of digital gene expression data. Bioinformatics 26: 139-140, 2010.
13. Korthauer K, Kimes PK, Duvallet C, Reyes A, Subramanian A, Teng M, Shukla C, Alm EJ and Hicks SC: A practical guide to methods controlling false discoveries in computational biology. Genome Biol 20: 118, 2019.
14. Ye Q, Liu J and Xie K: Zinc finger proteins and regulation of the hallmarks of cancer. Histol Histopathol 34: 1097-1109, 2019.
15. Wang J, Chitsaz F, Derbyshire MK, Gonzales NR, Gwadz M, Lu S, Marchler GH, Song JS, Thanki N, Yamashita RA, *et al*: The conserved domain database in 2023. Nucleic Acids Res 51: D384-D388, 2023.
16. Lu S, Wang J, Chitsaz F, Derbyshire MK, Geer RC, Gonzales NR, Gwadz M, Hurwitz DI, Marchler GH, Song JS, *et al*: CDD/SPARCLE: The conserved domain database in 2020. Nucleic Acids Res 48: D265-D268, 2020.
17. Marchler-Bauer A, Bo Y, Han L, He J, Lanczycki CJ, Lu S, Chitsaz F, Derbyshire MK, Geer RC, Gonzales NR, *et al*: CDD/SPARCLE: Functional classification of proteins via subfamily domain architectures. Nucleic Acids Res 45: D200-D203, 2017.
18. Lehmann W, Mossmann D, Kleemann J, Mock K, Meisinger C, Brummer T, Herr R, Brabletz S, Stemmler MP and Brabletz T: ZEB1 turns into a transcriptional activator by interacting with YAP1 in aggressive cancer types. Nat Commun 7: 10498, 2016.
19. Qin X, Zhou K, Dong L, Yang L, Li W, Chen Z, Shen C, Han L, Li Y, Chan AKN, *et al*: CRISPR screening reveals ZNF217 as a vulnerability in high-risk B-cell acute lymphoblastic leukemia. Theranostics 15: 3234-3256, 2025.
20. Enesa K and Evans P: The biology of A20-like molecules. Adv Exp Med Biol 809: 33-48, 2014.
21. Lee JH, Jung SM, Yang KM, Bae E, Ahn SG, Park JS, Seo D, Kim M, Ha J, Lee J, *et al*: A20 promotes metastasis of aggressive basal-like breast cancers through multi-monoubiquitylation of Snail1. Nat Cell Biol 19: 1260-1273, 2017.
22. Li J, Zhou Q, Zhang C, Zhu H, Yao J and Zhang M: Development and validation of novel prognostic models for zinc finger proteins-related genes in soft tissue sarcoma. Aging (Albany NY) 15: 3171-3190, 2023.
23. Wu P, Lin Y, Dai F, Wang H, Wen H, Xu Z, Sun G and Lyu Z: Pan-cancer analysis and experimental validation revealed the prognostic role of ZNF83 in renal and lung cancer cohorts. Discov Oncol 16: 1335, 2025.
24. Kou H, Jiang S, Wu X, Jing C, Xu X, Wang J, Zhang C, Liu W, Gao Y, Men Q, *et al*: ZNF655 involved in the progression of multiple myeloma via the activation of AKT. Cell Biol Int 49: 177-187, 2025.
25. Gan SY, Tye GJ, Chew AL and Lai NS: Current development of Fc gamma receptors (FcγRs) in diagnostics: A review. Mol Biol Rep 51: 937, 2024.
26. Rajasekaran N, Chester C, Yonezawa A, Zhao X and Kohrt HE: Enhancement of antibody-dependent cell mediated cytotoxicity: A new era in cancer treatment. Immunotargets Ther 4: 91-100, 2015.
27. Omori T, Machida T, Ishida Y, Sekiryu T and Sekine H: Roles of MASP-1 and MASP-3 in the development of retinal degeneration in a murine model of dry age-related macular degeneration. Front Immunol 16: 1566018, 2025.
28. Roumenina LT, Daugan MV, Petitprez F, Sautès-Fridman C and Fridman WH: Context-dependent roles of complement in cancer. Nat Rev Cancer 19: 698-715, 2019.

29. Merle NS and Roumenina LT: The complement system as a target in cancer immunotherapy. Eur J Immunol 54: e2350820, 2024.
30. Wess J: Designer GPCRs as novel tools to identify metabolically important signaling pathways. Front Endocrinol (Lausanne) 12: 706957, 2021.
31. Inverso D, Tacconi C, Ranucci S and De Giovanni M: The power of many: Multilevel targeting of representative chemokine and metabolite GPCRs in personalized cancer therapy. Eur J Immunol 54: e2350870, 2024.
32. Chen CL, Syahirah R, Ravala SK, Yen YC, Klose T, Deng Q and Tesmer JJG: Molecular basis for Gβγ-mediated activation of phosphoinositide 3-kinase γ. Nat Struct Mol Biol 31: 1198-1207, 2024.
33. Romeo Y and Roux PP: Paving the way for targeting RSK in cancer. Expert Opin Ther Targets 15: 5-9, 2011.
34. Chatterjee P, Ghosh D, Chowdhury SR and Roy SS: ETS1 drives EGF-induced glycolytic shift and metastasis of epithelial ovarian cancer cells. Biochim Biophys Acta Mol Cell Res 1871: 119805, 2024.
35. Nussinov R, Yavuz BR and Jang H: Molecular principles underlying aggressive cancers. Signal Transduct Target Ther 10: 42, 2025.
36. Du R, Shen W, Liu Y, Gao W, Zhou W, Li J, Zhao S, Chen C, Chen Y, Liu Y, *et al*: TGIF2 promotes the progression of lung adenocarcinoma by bridging EGFR/RAS/ERK signaling to cancer cell stemness. Signal Transduct Target Ther 4: 60, 2019.
37. Asghar J, Latif L, Alexander SPH and Kendall DA: Development of a novel cell-based, In-Cell Western/ERK assay system for the high-throughput screening of agonists acting on the delta-opioid receptor. Front Pharmacol 13: 933356, 2022.
38. Caunt CJ, Sale MJ, Smith PD and Cook SJ: MEK1 and MEK2 inhibitors and cancer therapy: The long and winding road. Nat Rev Cancer 15: 577-592, 2015.
39. Tian T, Li X and Zhang J: mTOR signaling in cancer and mTOR inhibitors in solid tumor targeting therapy. Int J Mol Sci 20: 755, 2019.
40. Mangé A, Coyaud E, Desmetz C, Laurent E, Béganton B, Coopman P, Raught B and Solassol J: FKBP4 connects mTORC2 and PI3K to activate the PDK1/Akt-dependent cell proliferation signaling in breast cancer. Theranostics 9: 7003-7015, 2019.
41. Al-Bari MAA and Xu P: Molecular regulation of autophagy machinery by mTOR-dependent and -independent pathways. Ann N Y Acad Sci 1467: 3-20, 2020.
42. Nowosad A, Jeannot P, Callot C, Creff J, Perchey RT, Joffre C, Codogno P, Manenti S and Besson A: Publisher correction: p27 controls ragulator and mTOR activity in amino acid-deprived cells to regulate the autophagy-lysosomal pathway and coordinate cell cycle and cell growth. Nat Cell Biol 23: 1048, 2021.
43. He K, Zheng X, Li M, Zhang L and Yu J: mTOR inhibitors induce apoptosis in colon cancer cells via CHOP-dependent DR5 induction on 4E-BP1 dephosphorylation. Oncogene 35: 148-157, 2016.
44. Karar J and Maity A: PI3K/AKT/mTOR pathway in angiogenesis. Front Mol Neurosci 4: 51, 2011.
45. Kim K, Kim IK, Yang JM, Lee E, Koh BI, Song S, Park J, Lee S, Choi C, Kim JW, *et al*: SoxF transcription factors are positive feedback regulators of VEGF signaling. Circ Res 119: 839-852, 2016.
46. Herrerias MM and Budinger GRS: Revisiting mTOR and epithelial-mesenchymal transition. Am J Respir Cell Mol Biol 62: 669-670, 2020.
47. Karimi Roshan M, Soltani A, Soleimani A, Rezaie Kahkhaie K, Afshari AR and Soukhtanloo M: Role of AKT and mTOR signaling pathways in the induction of epithelial-mesenchymal transition (EMT) process. Biochimie 165: 229-234, 2019.
48. Tian F, Yang X, Liu Y, Yuan X, Fan T, Zhang F, Zhao J, Lu J, Jiang Y, Dong Z and Yang Y: Constitutive activated STAT3 is an essential regulator and therapeutic target in esophageal squamous cell carcinoma. Oncotarget 8: 88719-88729, 2017.
49. D'Amico S, Shi J, Martin BL, Crawford HC, Petrenko O and Reich NC: STAT3 is a master regulator of epithelial identity and KRAS-driven tumorigenesis. Genes Dev 32: 1175-1187, 2018.
50. Andersson EI, Brück O, Braun T, Mannisto S, Saikko L, Lagström S, Ellonen P, Leppä S, Herling M, Kovanen PE and Mustjoki S: *STAT3* mutation is associated with STAT3 activation in $CD30^+$ ALK^- ALCL. Cancers (Basel) 12: 702, 2020.
51. Groner B and von Manstein V: Jak Stat signaling and cancer: Opportunities, benefits and side effects of targeted inhibition. Mol Cell Endocrinol 451: 1-14, 2017.
52. Sadrkhanloo M, Entezari M, Orouei S, Ghollasi M, Fathi N, Rezaei S, Hejazi ES, Kakavand A, Saebfar H, Hashemi M, *et al*: STAT3-EMT axis in tumors: Modulation of cancer metastasis, stemness and therapy response. Pharmacol Res 182: 106311, 2022.
53. Moreno L and Gatheral T: Therapeutic targeting of NOD1 receptors. Br J Pharmacol 170: 475-485, 2013.
54. Zhang W and Wang Y: Activation of RIPK2-mediated NOD1 signaling promotes proliferation and invasion of ovarian cancer cells via NF-κB pathway. Histochem Cell Biol 157: 173-182, 2022.
55. Taniguchi K and Karin M: NF-κB, inflammation, immunity and cancer: Coming of age. Nat Rev Immunol 18: 309-324, 2018.